Hindawi
Advances in Civil Engineering
Volume 2019, Article ID 9343917, 12 pages
https://doi.org/10.1155/2019/9343917

Research Article

A Water-Rock Coupled Model for Fault Water Inrush: A Case Study in Xiaochang Coal Mine, China

Luyuan Wu,[1] **Haibo Bai**,[1] **Chao Yuan**,[2] **Guangming Wu**,[1] **Changyu Xu**,[1] **and Yue Du**[1]

[1]*State Key Laboratory for Geo Mechanics and Deep Underground Engineering, China University of Mining and Technology, Xuzhou 221116, Jiangsu, China*
[2]*Department of Architecture and Civil Engineering, Xi'an University of Science and Technology, Xi'an 710054, Shaanxi, China*

Correspondence should be addressed to Haibo Bai; hbbai@126.com

Received 25 November 2018; Accepted 25 February 2019; Published 27 March 2019

Academic Editor: Hossein Moayedi

Water inrush disasters in mining frequently occur under the influence of confined water-bearing fault zones. Therefore, investigating the fault water inrush mechanism is necessary to reduce the number of occurrences of this type of disaster. In fault zones, the rock is highly fractured, and the mechanism of water conduction is complex. In this research, the seepage mechanism of fractured sandstone in fault zones is studied through experiments, and the results indicate that the permeability coefficient of fractured sandstone depends on the axial stress and particle size. The relationship between the permeability coefficient and axial stress was an exponential relationship. Then, a water-rock coupled model is proposed based on the experimental results, which considers the different water flow patterns during water inrush disasters. Finally, a numerical simulation combined with the water-rock coupled model is conducted to investigate the fault water inrush mechanism of a case study, and the results reveal that when water inrush disasters occur during mining, two types of conditions are required. One is that the connection among the fractured zone of the coal seam roof, fault fracture zone, and aquifer fails, and the other is that the connection among the fractured zone of the water inrush prevention pillar, fault fracture zone, and aquifer fails. This study contributes to an increased understanding of the mechanism of water inrush disasters and the design of water inrush prevention pillars.

1. Introduction

Fault zones are the outcome of active tectonic movement that occurs for a long period of time; fault zones have the following characteristics: (1) there are a large number of fracture surfaces in the fault fracture zone; (2) there is a lack of integrity and association between the structural fracture surfaces and rock mass that can easily result in flow deformation; (3) highly developed fractures are present, and the rock is highly fragmented in the fracture zone. Because of these characteristics, sufficient space is created for the confined water to flow along fault zone fractures. Moreover, fault zones often isolate confined water-bearing rock strata from coal seams. As a result, the aforementioned fault zones can act as water inrush channels between the confined water-bearing strata and adjacent working faces in the mine [1, 2]; the latter can easily result in water inrush accidents if no preventative measures are implemented. Figure 1 clarifies the above statements.

Therefore, it is necessary to study the water inrush mechanism between a confined water-bearing seam and coal seam working face in the presence of adjacent faults that contain water to reduce the number of water inrush accidents. Several researchers have considered water inrush disasters to be the result of water and rock interactions during mining. Li et al. [3] proposed that an excessive amount of fracture displacement and fault seepage erosion, which is caused by confined water in key layers of fault zones, constitute the floor water inrush mechanism of fault zones based on a structural layer model. Li et al. [4] proposed an activation mechanics model for the water-separated layer with faults based on the principle of a water-bearing layer. However, the aforementioned researchers did not consider the water-weakening effect, in that the compressive strength of rock containing water becomes lower than that of rock without water; in addition, the influence degree was related to the moisture content of the rock [5]. The water-weakening

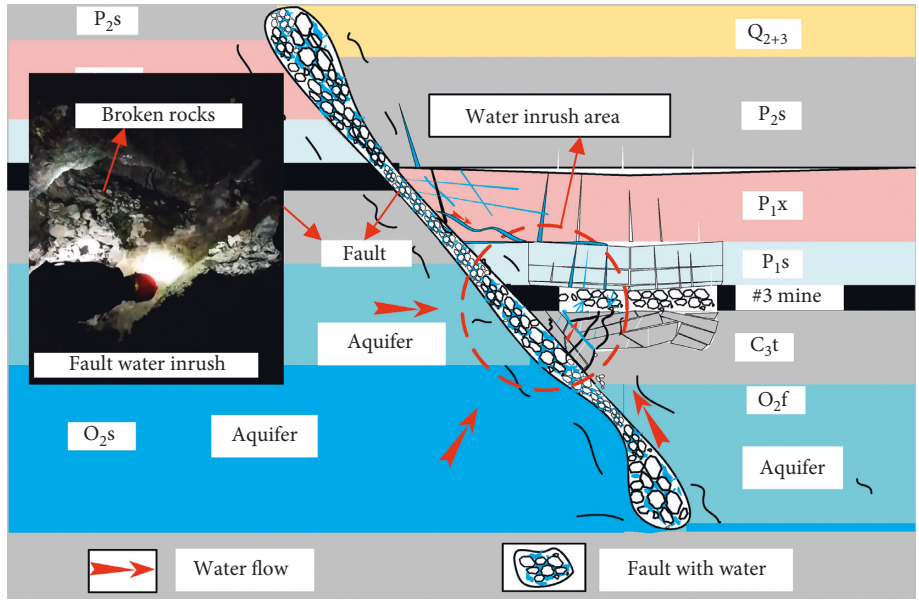

Figure 1: Description about fault water inrush in mining.

effect on different types of rocks has also been studied by numerous researchers [6–10], and certain experiments have also been conducted to investigate the water-rock interaction effects on the mechanical and seepage properties of rocks [11–13]. Terzaghi pioneered the theory of the effective stress of saturated soils with regards to the mechanical effect of water acting on rocks, where the effective stress was defined as the difference between the total stress and the pore water pressure as follows:

$$\sigma'_{ij} = \sigma_{ij} - \alpha p \delta_{ij}, \tag{1}$$

where σ_{ij} is the total stress, p is the pore water pressure, σ'_{ij} is the effective stress, δ_{ij} is the Kronecker symbol, and α is the effective stress coefficient. Since then, effective stress principles have been widely applied by several scholars as part of the fluid-solid coupled theory [14–18]. The Darcy law explains the flow of water in rocks with regards to the effect of rocks on water, and since then, other scholars have conducted numerous studies on the relationships among the pore pressure (pp), permeability coefficient, and strain and stress [13, 17, 19, 20]. In addition, numerous simulation studies have been performed to address water inrush issues [4, 15, 21–24]. However, these studies regarded the fault only as a discrete face, thereby neglecting the fault fracture zone and the water-rock coupling effect. Certain experiments and studies have also been conducted to investigate the seepage properties of fractured rocks [25–30]; however, the seepage properties were not associated with the fault water inrush mechanism. In addition, these investigations were mainly focused on continuous and quasi-continuous media and neglected the presence of a water-bearing fault in the mining zone; the physical and mechanical properties of rocks and rock masses are greatly affected and different from those of rocks and rock masses without faults. Furthermore, these investigations focused on an analysis of the mechanics, and only a few focused on the fault water inrush mechanism considering the water-rock coupled theory. The limitations are as follows: fault water inrush investigations focused on the stress analysis of the surrounding rock without considering the influence of the seepage field; the evolution of fault water inrush channels was not clearly represented in the mining process adjacent to a fault zone; and at the same time, the percolation evolution of fractured rock in the fault fracture zone has rarely been studied. In contrast to other studies, this paper investigates the percolation evolution of fractured rock in the fault fracture zone through experiments. Then, a water-rock coupled model is established and the evolution of fault water inrush channels is investigated through numerical simulation.

2. Research Methodology

The research methodology is shown in Figure 2. First, the seepage mechanism of fractured rock in the fault fracture zone is studied through experiments. The experimental steps are shown in Figure 2(a). Second, the water-rock coupled model is extended based on the experimental results, and the water-rock coupled process is proposed, as shown in Figure 2(b). Third, numerical simulation is conducted to analyze the fault water inrush process, and the calculation process is shown in Figure 2(c). The research methods are introduced in the following sections.

2.1. Seepage Experiments of Fractured Rock

2.1.1. Sample Preparation. Samples were taken from the Mount Er Gang fault in the Xiao Chang coal mine in Changzhi city, Shanxi Province, China. The drilling locations of the samples are adjacent to the fault (Figure 3). The drilled samples were sandstone, which were relatively fractured (Figure 4). The samples were ground to obtain a smaller particle size and then graded using grading sieves.

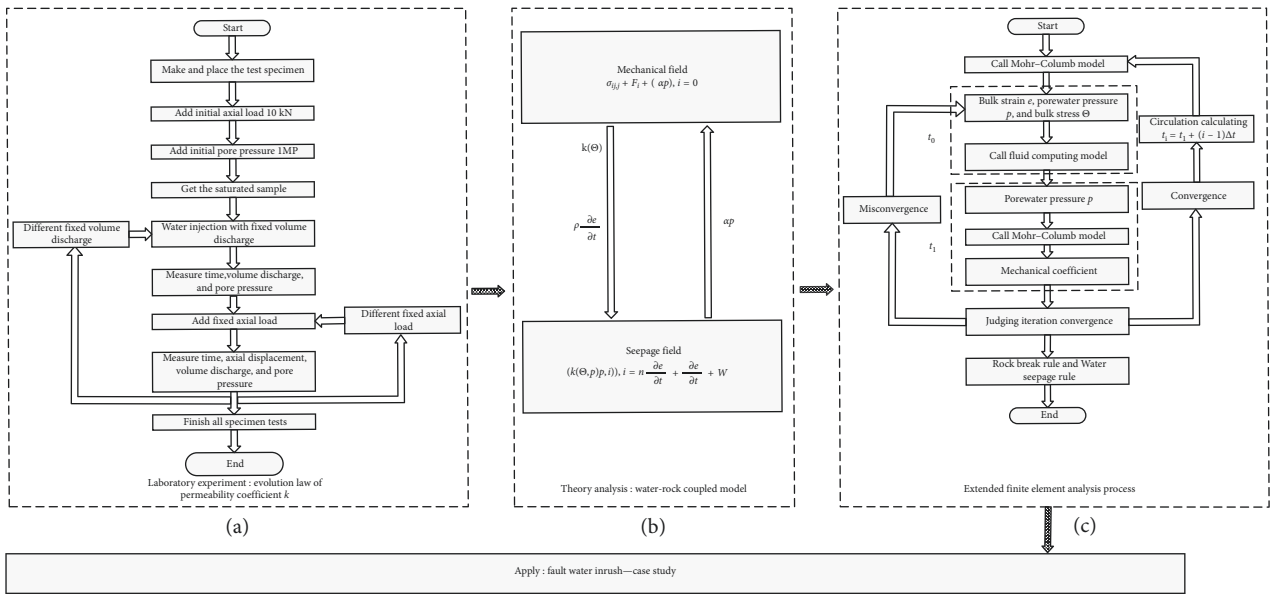

Figure 2: The research process of the paper

The particle size ranges of each grade were size 1 (5–10 mm), size 2 (10–15 mm), size 3 (15–20 mm), and size 4 (20–26.5 mm), which are shown in Figure 4. Three groups of specimens were prepared for each particle size range to ensure that the experimental results were representative.

2.1.2. Experimental Programme. An MTS815.02 electrohydraulic servo controller rock mechanics testing system and a self-regulating seepage apparatus were used in the test, and the experimental apparatus components are shown in Figure 5. The apparatus could not only conduct steady penetration experiments but could also conduct transient penetration experiments. However, the pore pressure difference between the circular sections of the specimen rapidly disappeared during the transient penetration experiment because of the high permeability of the fractured medium. Hence, a steady-state experiment was conducted. The load was controlled below 20 kN after preparing and installing the samples, and the pore pressure did not exceed 0.5 MPa under the influence of open water circulation control; as a result of the latter, the medium was fully saturated. Then, the test equipment was loaded automatically according to the design procedure. Detailed experimental steps are shown in Figure 2. The seepage calculation of the fractured sandstone experiment is shown below; with regards to the steady-state experiment, the permeability coefficient was calculated with the Darcy law as follows (equation (2)):

$$k = \frac{v}{J},$$

$$v = \frac{q}{A_s}, \tag{2}$$

$$J = \frac{l}{h_1 - h2},$$

where k is the permeability of samples, v is the seepage velocity, q is the quantity, A_s is the cross-sectional area of the samples, l is the length of the samples, h_1 and h_2 represent the waterhead, and J is the hydraulic gradient. Moreover, to evaluate whether the seepage was in agreement with Darcy seepage, the Reynolds number was calculated with the following equation:

$$R_e = \frac{\rho \cdot q}{\gamma_w A_s} d, \tag{3}$$

where R_e is the Reynolds number, d is the particle diameter, and γ_w is the water kinematic viscosity. Hence, $R_{e\,\max}$ was 0.44 as calculated by using equations (2) and (3), which confirmed that the seepage observed during the experiment was the Darcy seepage.

(1) Analysis experimental results: the experimental results with regards to the relationship between k and axial stress σ of sandstone consisting of different particle sizes are shown in Figures 6(a)–6(d).

From the abovementioned diagrams, the following conclusions could be drawn: (1) given the same axial stress, the smaller the particle was, the smaller the permeability coefficient was; (2) the flow rate of water had little effect on the permeability coefficient, which increased slightly with increasing flow rate; (3) the permeability coefficient of fractured sandstone was much higher than that of intact sandstone under the action of axial stress; and (4) the fractured rock became compacted, and the permeability coefficient decreased as the axial stress increased. Moreover, the relationship between the permeability coefficient and axial stress was nonlinear, so an exponential function (equation (4)) was used to describe the nonlinear relationship. The relationship between the experimental permeability coefficient k and axial stress σ is shown in Figures 6(a)–6(d) and represented as follows:

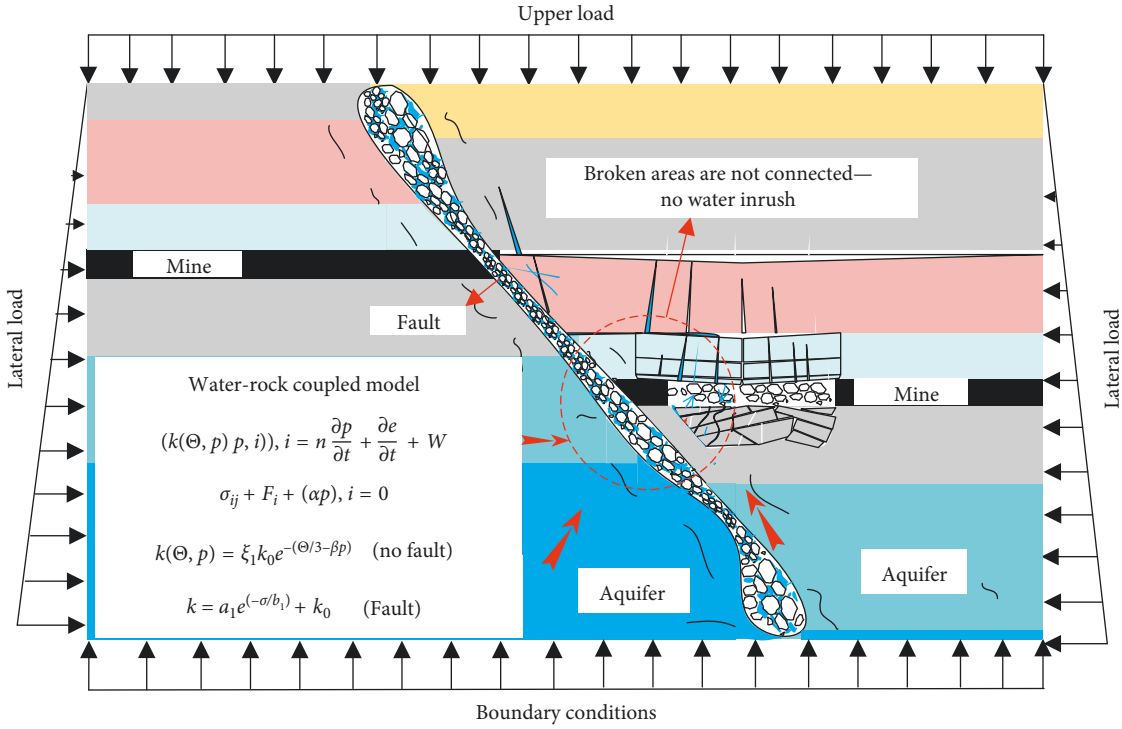

Figure 3: Water-rock coupled calculation models. (a) Model I; (b) Model II

$$k = a_1 e^{(-\sigma/b_1)} + k_0, \tag{4}$$

where a_1 and b_1 are coefficients related to the particle size, whose values are shown in Table 1, and k_0 is the initial permeability coefficient.

2.2. Water-Rock Coupled Model

2.2.1. Rock Stress Analysis. The elastic-plastic mechanical constitutive relationship of a rock mass under the coupled effect of stress and seepage fields is described by using

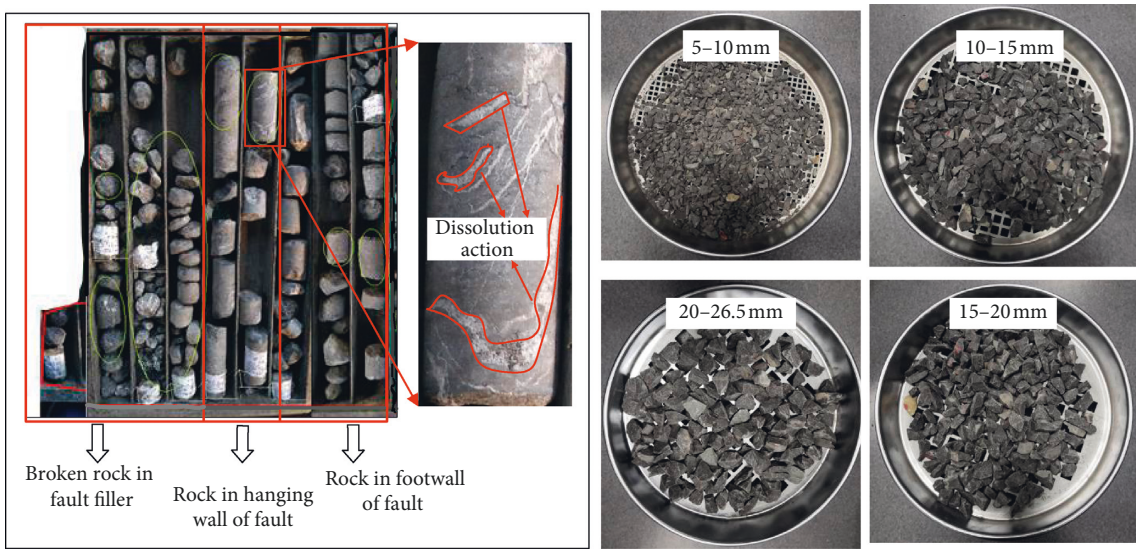

Figure 4: Sample preparation.

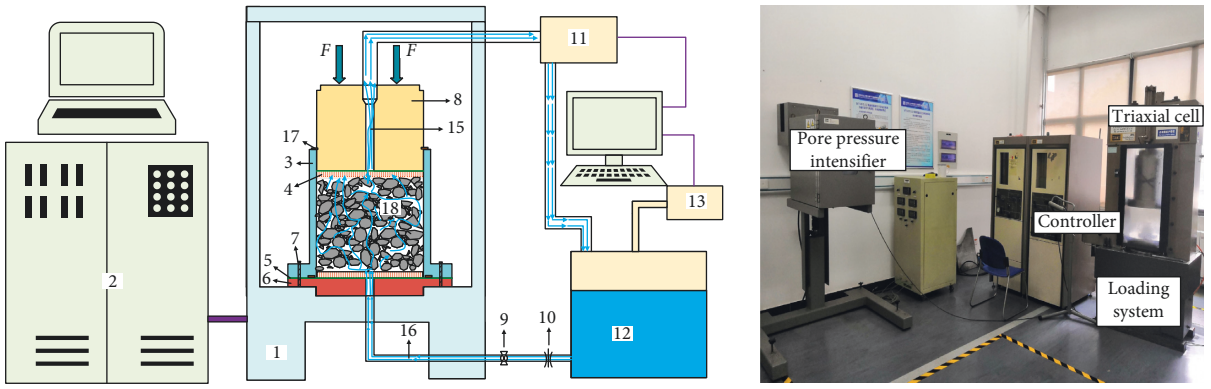

(1) and (2) MTS815.02 electrohydraulic servo controller rock mechanics
(3) Sleeve
(4) Porous disc
(5) Felt
(6) Pedestal
(7) Bolted joint
(8) Piston
(9) Ball valve
(10) Flow regulator
(11) Outflow measure
(12) Water supply system
(13) Water pressure monitoring and control system
(14) Information processing system
(15) Water outflow channel
(16) Water inflow channel
(17) Sleeve seal ring
(18) Samples

(a) (b)

Figure 5: Testing system of the seepage evolution law.

equation (5) in which the Mohr–Coulomb strength criterion is treated as the yield criterion. The element shear and element stretch fracturing conditions are given in equations (6) and (7), which consider the water-weakening effect on the rock compressive strength, as follows:

$$\sigma_{ij,j} + F_i + (\alpha p), \quad i = 0, \tag{5}$$

$$f_s = \tau - \eta_s (c + \sigma tg\varphi) = 0, \tag{6}$$

$$f_t = \sigma_t - \frac{2c \cdot \cos\varphi}{1 + \sin\varphi} = 0, \tag{7}$$

where $\sigma_{ij,j}$ is the total stress tensor, αp is the osmotic hydraulic gradient expressed as the force of an equivalent volume applied to the rock mass skeleton, F_i is the applied load, and η_s is the rock shear strength weakening coefficient and $\eta_s = 0.759$ [28].

2.2.2. Seepage Analysis. The seepage differential control equation can be provided as follows:

$$(k(\Theta, p)p, i)), i = n\frac{\partial p}{\partial t} + \frac{\partial e}{\partial t} + W, \tag{8}$$

where p is the pore water pressure, e is the volume deformation, W is the water source, t is the time, and k is the permeability coefficient, which can be calculated with the following equation [17]:

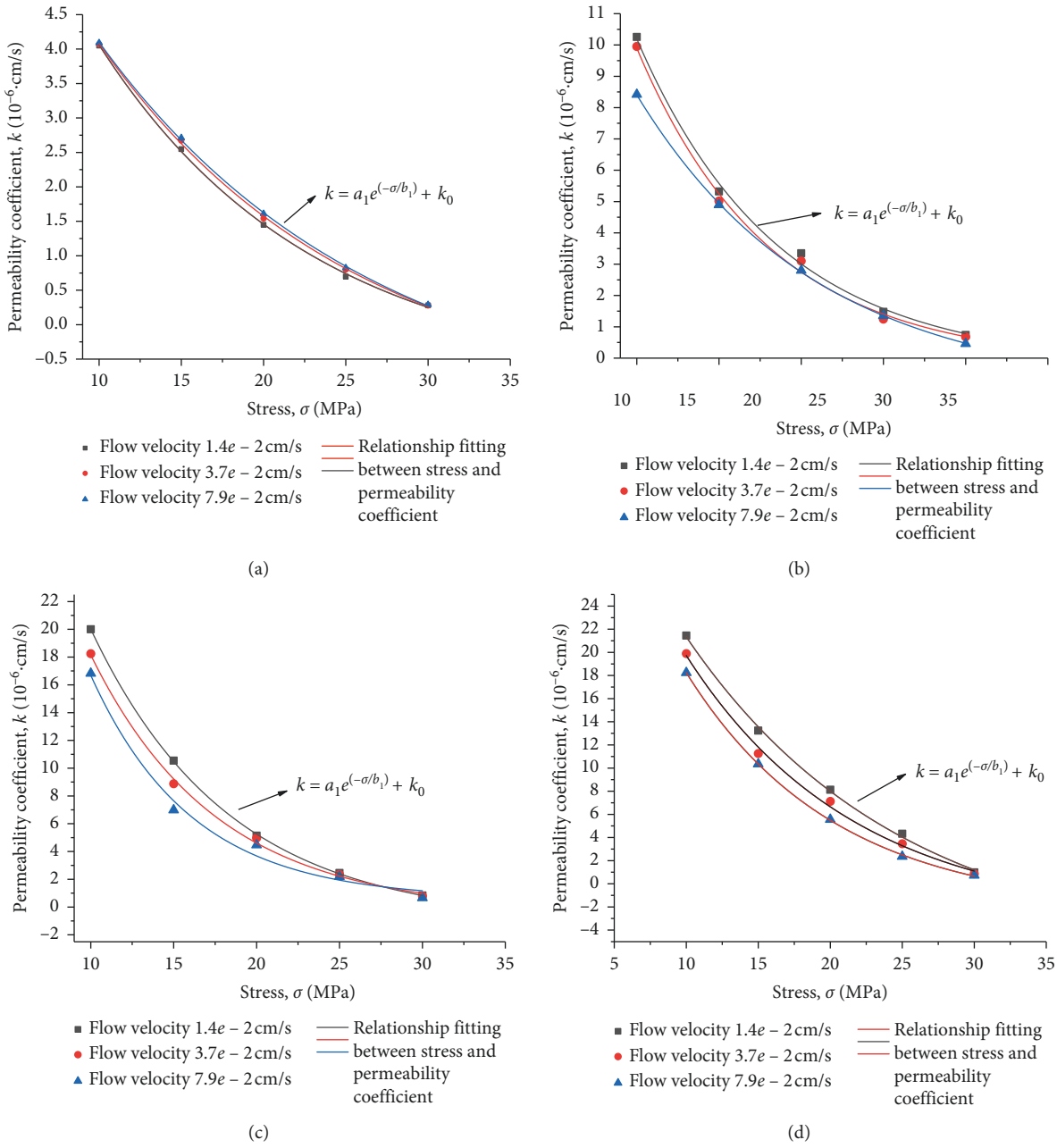

Figure 6: Particle diameter: (a) 5 mm–10 mm; (b) 10 mm–15 mm; (c) 15 mm–20 mm; (d) 20 mm–26.5 mm.

Table 1: Values of a_1 and b_1 in equation (4).

	Particle size			
	2–5 mm	5–11 mm	11–16 mm	16–22 mm
a_1	10.05863	34.83086	69.21798	53.50645
b_1	13.96715	8.04681	7.57432	11.68213

$$k(\Theta, p) = \xi_1 k_0 e^{-(\Theta/3-\beta p)}, \quad (9)$$

where $\xi_1 = 1.0$ and $\beta = 0.5$ for nonfractured surrounding rock, $\xi_1 = 1000$ and $\beta = 1.0$ for fractured surrounding rock, Θ is the volume stress, $\Theta = \sigma_1 + \sigma_2 + \sigma_3$, and e is the volume strain, which is subject to $e = \varepsilon_1 + \varepsilon_2 + \varepsilon_3$.

The permeability coefficient of the fractured rock mass of the fault zone is calculated with equation (4). The evaluation of the stress and seepage could be investigated with water-rock coupled model I, which is shown in Figure 3(a); the figure shows that the fractured zone of the coal seam roof, coal seam floor, and fault were interconnected, and water inrush occurred during mining of the coal seam. The nonlinear water flow in the water inrush channel could be represented by using the Darcy–Weisbach equation (10) if the fractured zone of the coal seam roof, water-bearing fault fracture zone, and confined aquifer were interconnected or if the fractured zone of the coal seam floor and water-bearing fault

fracture zone were interconnected; water flowed into the goaf though the water inrush channel:

$$\Delta H = f \cdot \frac{l}{\overline{d}} \cdot \frac{u^2}{2g}, \tag{10}$$

where ΔH is the waterhead loss, l is the length of the water inrush channel, $\overline{d}$ is the inner diameter of the water inrush channel, u is the average velocity in the channel, g is the gravity acceleration, and f is the friction coefficient (dimensionless), whose value can be calculated based on the Nikuradse experiment curve as shown below:

$$f = \begin{cases} \dfrac{1}{[1.74 + 2\lg(2\Delta/d)]^2}, & \mathrm{Re} > 100000, \\ \dfrac{64}{R_e}, & \mathrm{Re} < 2300, \\ \dfrac{0.326}{R_e^{0.25}}, & 2300 < \mathrm{Re} < 100000. \end{cases} \tag{11}$$

If the voidage of the water inrush channel is 1, then $v = u$ and $J = \Delta H/l$, and the following relationship can be acquired based on equation (10) [31]:

$$v = \frac{2gd}{fv} \cdot J. \tag{12}$$

Then, an equivalent permeability coefficient K_d can be calculated with equation (12), where v is the water velocity:

$$K_d = \frac{2gd}{fv}. \tag{13}$$

Therefore, the water inrush process could be approximated by a nonlinear seepage equation after water inrush was generated and occurred. The evolution of stress and seepage could be investigated by water-rock coupled model II, which is shown in Figure 3(b).

3. Case Study

3.1. Engineering Background. The Xiao Chang coal mine is located in the Xiao Chang field, Changzhi city, Shanxi Province, China. The southern normal fault of the Mount Er Gang is the western boundary of the Xiao Chang mine and the boundary fault of the mine; the other geological conditions are shown in Figure 7. The fault contains water and cuts off the #3 coal seam. As a result of the stratigraphic throw reaching 300 m, the #3 coal seam in the upper part of the southern normal fault of the Mount Er Gang is directly connected with the Ordovician water-bearing rock stratum in the lower part of the fault, as shown in Figure 1.

Working face 30225 with adjacent faults will be mined and the water-bearing fault zone. If the fractured zone of the floor, roof, reserved coal pillar, fault zone, and surrounding rock are interconnected during mining of the coal seam, water inrush accidents will occur; the mining situation is shown in Figure 1. Therefore, when coal seams with adjacent faults that contain water are mined, it is necessary to study the water inrush mechanism between the confined water-bearing rock stratum and mining work face for the prevention and control of water inrush.

3.2. Numerical Simulation of the Water Inrush Process. Numerical simulation was performed to investigate the water inrush mechanism of coal seam mining with adjacent faults that contain water at the Xiao Chang coal mine, and the simulated location is shown in Figure 7. The constitutive calculation model described in Section 2 was used for the numerical simulations based on the geological conditions shown in Figure 2(c). The numerical simulation results are shown in Figures 8–10.

Figure 8(a) shows that the mining process disturbed the stress field of the surrounding rock during mining of the coal seam, and when the mining width reached 40 m, the rocks within the fault zone and surrounding rock above the fault had fractured. Furthermore, the fractured zone of the roof and floor of the coal seam expanded gradually with increasing mining width. As shown in Figure 8(b), when the mining width reached 140 m, the water inrush prevention pillar was destroyed as a result of damage and stress concentration effects in the rock surrounding the fault zone caused by mining. The latter contributed to the flow of water from the confined aquifer to the fault zone, then to the reserved water inrush prevention pillar, and finally to the gob, which created the conditions to form a water inrush channel. In addition, although there was no connection between the destroyed roof zone and the fault activation zone, the aforementioned zones had a tendency to become interconnected. Since water always flows from high to low potential energy, the change in pore water pressure could reflect the flow of water. Based on the pore water pressure isoline distribution (Figure 9), fault water inrush to the gob occurred under the action of a high hydraulic gradient as the mining width reached 140 m, and the first water inrush channel (aquifer-fault zone-reserved water inrush prevention pillar-gob zone) was generated; the latter is shown and labelled in Figure 9. Furthermore, the flow variation in the monitoring element #1 also indicated that the process of water inrush had occurred, which is shown in Figure 11. When the mining width reached 100 m, the water flow was 7.056 m^3/h and increased gradually; when the fault width reached 140 m, the water flow increased abruptly to 331.632 m^3/h, and when the mining width reached 180 m, the water flow reached a maximum value of 749.916 m^3/h; thereafter, the water flow decreased gradually, which was caused by the sudden release of water potential energy after formation of the first water inrush channel.

When the mining width reached 170 m, the fractured zone of the coal seam roof connected with the fault fracture zone, as shown in Figure 8(c), and created conditions suitable for the flow of water to occur from the water-bearing strata to the gob through the fault and fractured zone of the roof and contributed to the formation of a second water inrush channel (confined aquifer-fault zone-faults surrounding the fractured rock zone-fractured roof zone-gob zone).

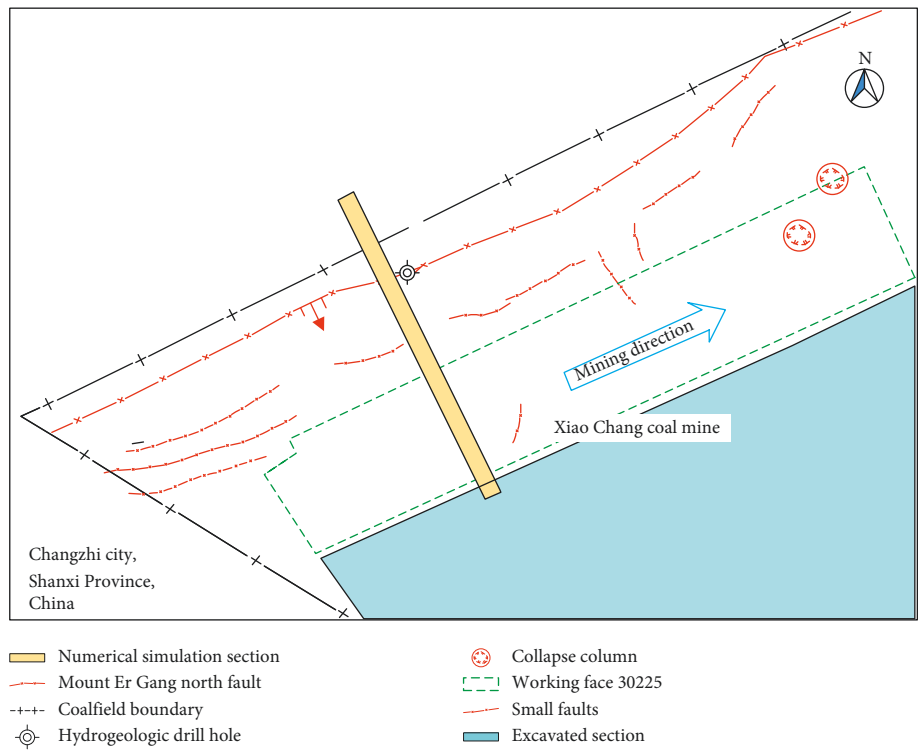

Figure 7: Engineering environment in Xiao Chang coal mine.

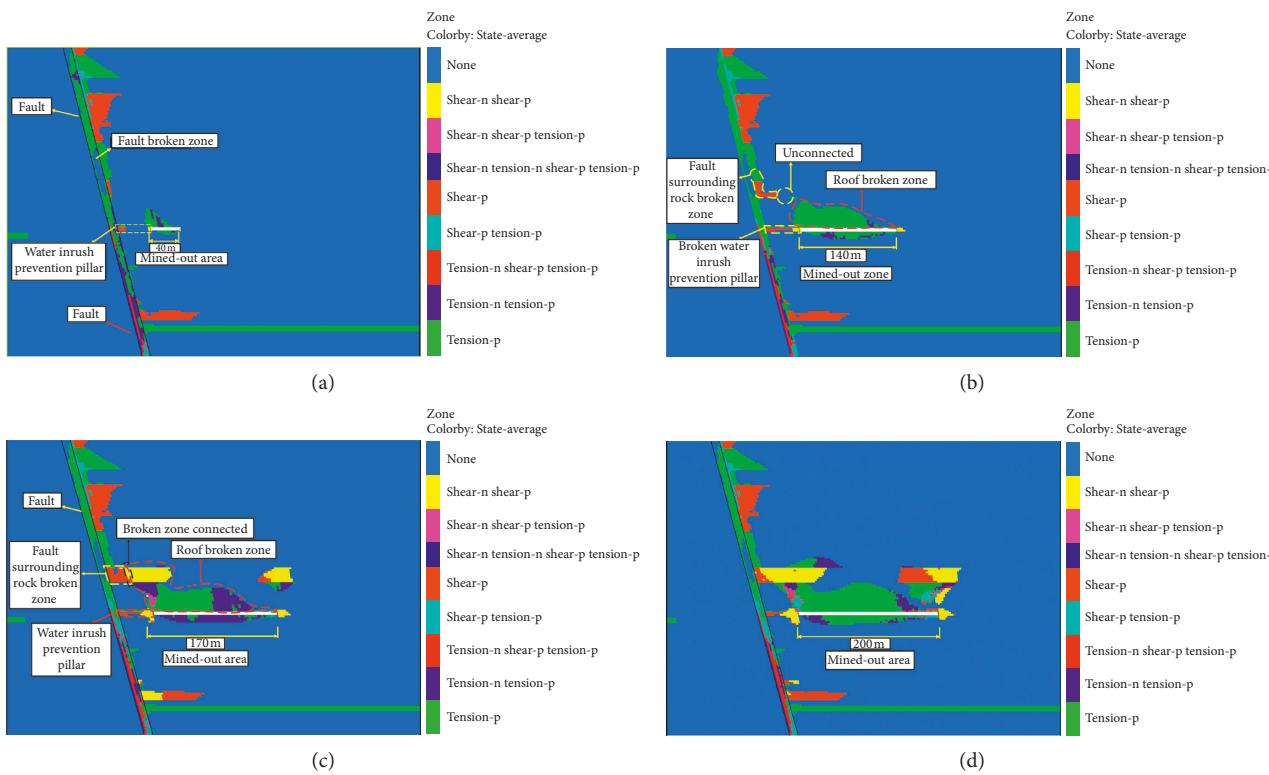

Figure 8: The evolution laws of broken zone caused by mining.

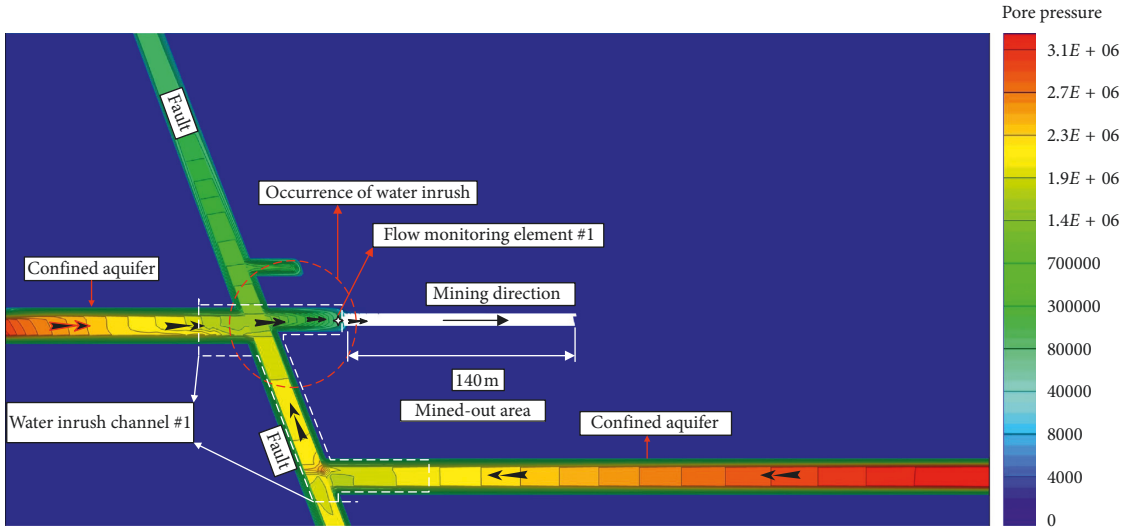

Figure 9: Pore pressure distribution when mining width reaches 170 m.

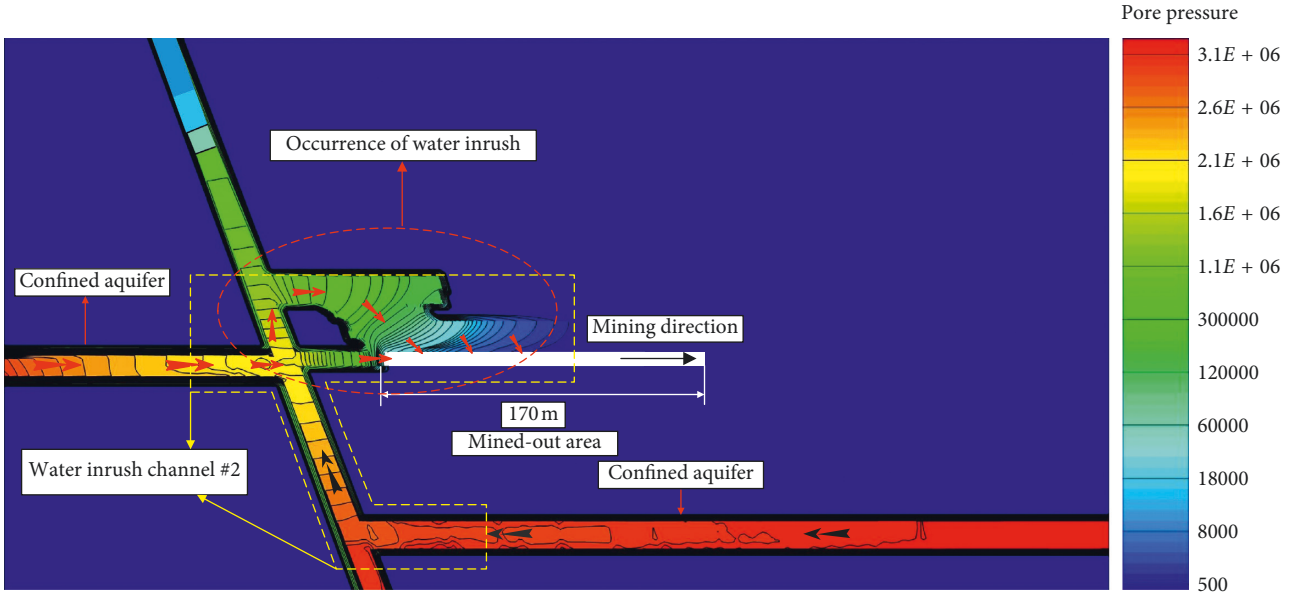

Figure 10: Pore pressure distribution when mining width reaches 170 m.

The second water inrush channel is reflected by the pore water pressure isoline distribution (Figure 10). The flow of water in the gob would increase greatly with the increase in the number of water inrush channels, which would result in great hazards to working face 30225. Hence, it was important to calculate and monitor the evolution of the fractured zone of the coal seam roof, floor, and water inrush prevention pillar to determine the water inrush mechanism. Furthermore, the flow variation in the monitoring element #2 also indicated that the process of water inrush had occurred at roof, which is shown in Figure 11. When the mining width reached 140 m, the water flow was 0.014 m^3/h and increased gradually; when the fault width reached 180 m, the water flow increased abruptly to 216.138 m^3/h, and when the mining width reached 220 m, the water flow reached a maximum value of 574.005 m^3/h; thereafter, the water flow decreased gradually, which was caused by the sudden release of water potential energy after formation of the second water inrush channel.

4. Discussion

This paper presented the water inrush mechanism in the mining process under engineering conditions where there was a water-bearing fault zone near the coal seam and a water-bearing fault zone connected with a confined aquifer.

4.1. Seepage Experiments of Fractured Rock. Since there was a large amount of fractured rocks in the fault zone, the seepage evolution mechanism of the fractured sandstone rock in the

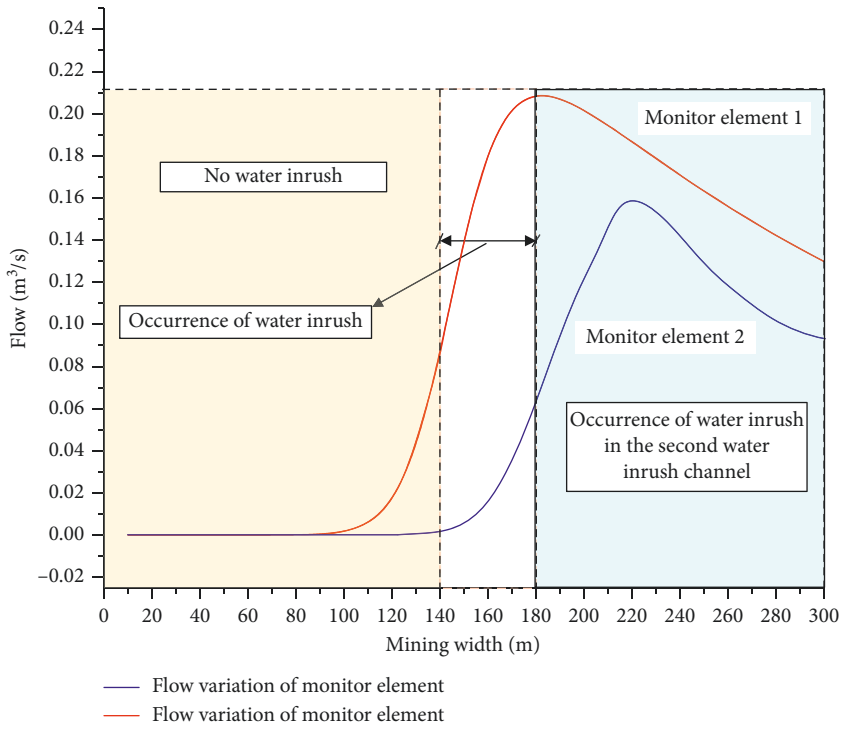

Figure 11: Flow variation of monitor element.

fault zone was investigated through experiments. We found that the flow rate of water had little effect on the permeability coefficient, which increased slightly with increasing flow rate; the permeability coefficient of fractured sandstone was much higher than that of intact sandstone under the action of axial stress; the fractured rock became compacted, and the permeability coefficient decreased as the axial stress increased. Moreover, the relationship between the permeability coefficient and axial stress was nonlinear, so an exponential function (equation (4)) was used to describe the nonlinear relationship. The other study results show that permeability parameter k of crushed rock has a polynomial relationship with effective stress σ' in inverse proportion [23, 25, 26, 28, 31, 32].

4.2. Water-Rock Coupled Model. Compared with previous studies [18, 33–35], the water-rock coupled model presented in this paper was different in that (1) the model considered the water-weakening effect on the rock strength; (2) the model relied on different seepage coefficients based on the different water flow patterns before and after water inrush occurred; and (3) different calculation models were adopted for different engineering conditions that better conformed to the actual situation. In other studies, the seepage character of fault broken zone is always ignored [17]. The disadvantage of the model is that we do not consider the influence of temperature and cannot calculate the analytical solution of the model. Furthermore, the experiment did not consider triaxial stress conditions, which means that the effect of the confining pressure on the permeability coefficient of the fractured rock mass was ignored in this study, which could be considered in the future by designing corresponding equipment. We hypothesized that fractured rock was a continuous medium. Therefore, evaluating the applicability of the water-rock coupled model is necessary in future research.

4.3. Numerical Simulation. The numerical simulation results of the fault water inrush process indicated that the connection among fractured zones is a prerequisite for the occurrence of a water inrush disaster during mining. In addition, there are two water inrush tunnels: the first water inrush channel (aquifer-fault zone-reserved water inrush prevention pillar-gob zone) and the second water inrush channel (confined aquifer-fault zone-faults surrounding the fractured rock zone-fractured roof zone-gob zone). However, scholars also need to pay attention to additional water inrush channels [9, 25, 36] for different geological conditions, including the condition where the aquifer-fault-floor fractured zone may also function as the water inrush channel.

5. Conclusions

This paper addressed the fault water inrush mechanism through seepage experiments with fractured rock samples from a fault zone, water-rock coupled models, and numerical simulations. The following conclusions were drawn:

(1) The flow rate of water had little effect on the permeability coefficient, which increased slightly with increasing flow rate; the permeability coefficient of fractured sandstone was much higher than that of intact sandstone under the action of axial stress; the

fractured rock became compacted, and the permeability coefficient decreased as the axial stress increased. Moreover, the relationship between the permeability coefficient and axial stress was nonlinear.

(2) Using different seepage coefficients based on the different water flow patterns before and after water inrush occurred resulted in the determination of the fault water inrush mechanism. Two water-rock coupled models are processed in the manuscript, and both models consider the seepage law of broken rock and whole rock. One is used in the situation where the broken areas do not interconnect, and the other is used in the situation where the broken area interconnects.

(3) The fault zone affected the fracture evolution of the coal seam roof, and the fractured zone of the adjacent fault became larger and wider than the other zone. The connection among the fractured zone of the coal seam roof, fault fracture zone, and aquifer, or among the fractured zone of the water inrush prevention pillar, fault fracture zone, and aquifer was a requirement for the occurrence of water inrush disasters during mining.

This study contributes an increased understanding of the mechanism of water inrush disasters and provides helpful suggestions for the design of water inrush prevention pillars.

Data Availability

All data generated or analyzed during the study are included in the published paper.

Conflicts of Interest

The authors declare that they have no conflicts of interest.

Acknowledgments

This work was supported by the National Natural Science Foundation of China (51323004) and the National Basic Research Program of China (2013CB227900).

References

[1] H. B. Bai, J. L. Yang, and C. S. Wang, "Research on limestone aquifuge in top Ordovician and its application in roadway excavated through graben faults," *Journal of Mining and Safety Engineering*, vol. 27, pp. 322–328, 2010.

[2] H. Bai, D. Ma, and Z. Chen, "Mechanical behavior of groundwater seepage in karst collapse pillars," *Engineering Geology*, vol. 164, pp. 101–106, 2013.

[3] L. J. Li, M. G. Qian, and S. G. Li, "Mechanism of water-inrush through fault," *Journal of China Coal Society*, vol. 45, pp. 119–124, 1996.

[4] L. T. Li, C. Tang, and Z. Z. Liang, "Numerical analysis of pathway formation of groundwater onrush from faults in coal seam floor," *Chinese Journal of Rock Mechanics and Engineering*, vol. 28, pp. 290–297, 2009.

[5] W. Tanikawa and T. Shimamoto, "Comparison of Klinkenberg-corrected gas permeability and water permeability in sedimentary rocks," *International Journal of Rock Mechanics and Mining Sciences*, vol. 46, no. 2, pp. 229–238, 2009.

[6] L. S. Burshtein, "Effect of moisture on the strength and deformability of sandstone," *Soviet Mining Science*, vol. 5, no. 5, pp. 573–576, 1969.

[7] D. Ma, H. Y. Duan, J. F. Liu, X. B. Li, and Z. L. Zhou, "The role of gangue on the mitigation of mining-induced hazards and environmental pollution: an experimental investigation," *Science of the Total Environment*, vol. 664, pp. 636–448, 2019.

[8] Z.-g. Ma, X.-x. Miao, F. Zhang, and Y.-s. Li, "Experimental study into permeability of broken mudstone," *Journal of China University of Mining and Technology*, vol. 17, no. 2, pp. 147–151, 2007.

[9] D. Ma, M. Rezania, H.-S. Yu, and H.-B. Bai, "Variations of hydraulic properties of granular sandstones during water inrush: effect of small particle migration," *Engineering Geology*, vol. 217, pp. 61–70, 2017.

[10] D. R. Simpson, J. H. Fergus, and H. Fergus, "The effect of water on the compressive strength of diabase," *Journal of Geophysical Research*, vol. 73, no. 20, pp. 6591–6594, 1968.

[11] D. Ma, X. Cai, Z. L. Zhou, and X. B. Li, "Experimental investigation on hydraulic properties of granular sandstone and mudstone mixtures," *Geofluids*, vol. 2018, Article ID 9216578, 13 pages, 2018.

[12] F. L. Pellet, M. Keshavarz, and M. Boulon, "Influence of humidity conditions on shear strength of clay rock discontinuities," *Engineering Geology*, vol. 157, pp. 33–38, 2013.

[13] T. Yang, W. Shi, S. Li, Y. Xin, and B. Yang, "State of the art and trends of water-inrush mechanism of nonlinear flow in fractured rock mass," *Journal of China Coal Society*, vol. 41, pp. 1598–1609, 2016.

[14] A. E. Bond, I. Bruský, T. Cao et al., "A synthesis of approaches for modelling coupled thermal–hydraulic–mechanical–chemical processes in a single novaculite fracture experiment," *Environmental Earth Sciences*, vol. 76, pp. 1–19, 2017.

[15] D. Ma, X. Cai, Q. Li, and H. Duan, "In-situ and numerical investigation of groundwater inrush hazard from grouted karst collapse pillar in longwall mining," *Water*, vol. 10, no. 9, p. 1187, 2018.

[16] Z. W. Qian, Z. Huang, and J. G. Song, "A case study of water inrush incident through fault zone in China and the corresponding treatment measures," *Arabian Journal of Geosciences*, vol. 11, no. 14, pp. 1–20, 2018.

[17] D. Ma, X. Miao, H. Bai et al., "Effect of mining on shear sidewall groundwater inrush hazard caused by seepage instability of the penetrated karst collapse pillar," *Natural Hazards*, vol. 82, no. 1, pp. 73–93, 2016.

[18] J. Zhang, W. B. Standifird, J. C. Roegiers, and Y. Zhang, "Stress-dependent fluid flow and permeability in fractured media: from lab experiments to engineering applications," *Rock Mechanics and Rock Engineering*, vol. 40, no. 3, pp. 3–21, 2007.

[19] S. Chaki, M. Takarli, and W. P. Agbodjan, "Influence of thermal damage on physical properties of a granite rock: porosity, permeability and ultrasonic wave evolutions," *Construction and Building Materials*, vol. 22, no. 7, pp. 1456–1461, 2008.

[20] J. Yu, H. Li, X. Chen, Y. Cai, N. Wu, and K. Mu, "Triaxial experimental study of associated permeability-deformation of sandstone under hydro-mechanical coupling," *Chinese*

Journal of Rock Mechanics and Engineering, vol. 32, pp. 1203–1213, 2013.

[21] L. P. Li, S. C. Li, S. S. Shi, and Z. H. Xu, "Water inrush mechanics study of fault activation induced by coupling effect of stress-seepage -seepage-damage," *Journal of Rock Mechanics and Engineering*, vol. 30, pp. 3296–3304, 2013.

[22] M. Z. Naghadehi, R. KhaloKakaie, and S. R. Torabi, "The influence of moisture on sandstone properties in Iran," *Proc Inst Civil Eng Geotech Eng*, vol. 16, pp. 91–99, 2010.

[23] L. Z. Wang, Z. Q. Chen, and H. L. Kong, "An experimental investigation for seepage-induced instability of confined broken mudstones with consideration of mass loss," *Geofluids*, vol. 2017, Article ID 3057910, 12 pages, 2017.

[24] Z. Zhou, X. Cai, D. Ma et al., "Water saturation effects on dynamic fracture behavior of sandstone," *International Journal of Rock Mechanics and Mining Sciences*, vol. 114, pp. 46–61, 2019.

[25] Q. F. Li, W. J. Wang, C. Q. Zhu, and W. Q. Peng, "Analysis of fault water-inrush mechanism based on the principle of water-resistant key strata," *Journal of Mining and Safety Engineering*, vol. 26, pp. 87–90, 2009.

[26] Z. H. Li, C. Z. Zhai, and L. F. Li, "Experimental study on water inrush mechanism due to floor faults activation in mining above confined aquifer," *Journal of Central South University (Science and Technology)*, vol. 46, pp. 1806–1811, 2015.

[27] Z. Zhou, X. Cai, D. Ma, L. Chen, S. Wang, and L. Tan, "Dynamic tensile properties of sandstone subjected to wetting and drying cycles," *Construction and Building Materials*, vol. 182, pp. 215–232, 2018.

[28] B. Vasarhelyi, "Staistical analysis of the influence of water content on the strength of the mi cene limestone," *Rock Mechanics and Rock Engineering*, vol. 38, pp. 69–76, 2005.

[29] L. K. Foong, N. A. Rahman, and R. Nazir, "Experimental study on unsaturated double-porosity soil phenomena under vibration effect," *Jurnal Teknologi*, vol. 79, no. 4, pp. 64–72, 2017.

[30] N. A. Rahman, L. K. Foong, R. Nazir, and R. W. Lewis, "Vibration effect influence upon non-aqueous phase liquid migration in double-porosity," *Geologia Croatica*, vol. 71, no. 3, pp. 163–171, 2018.

[31] Y. Zhang, W. Y. Xu, J. F. Shao, H. B. Zhao, W. Wang, and S. H. Mei, "Experimental investigation on rheological Properties and permeability of clastic rock under hydro-mechanical coupling," *Chinese Journal of Rock Mechanics & Engineering*, vol. 33, pp. 1679–1690, 2014.

[32] L. K. Foong, N. A. Rahman, R. Nazir, R. Sa'ari, and M. Mustaffar, "Investigation of aqueous and non-aqueous phase liquid migration in double-porosity soil using digital image analysis," *Journal of Chemical Engineering Transactions (AIDIC)*, vol. 63, pp. 685–690, 2018.

[33] D. Ma, H. Duan, X. Cai, Z. Li, Q. Li, and Q. Zhang, "A global optimization-based method for the prediction of water inrush hazard from mining floor," *Water*, vol. 10, no. 11, p. 1618, 2018.

[34] V. N. Odintsev and N. A. Miletenko, "Water inrush in mines as a consequence of spontaneous hydrofracture," *Journal of Mining Science*, vol. 51, no. 3, pp. 423–434, 2015.

[35] Y. Xue, D. Wang, S. Li, D. Qiu, Z. Li, and J. Zhu, "A risk prediction method for water or mud inrush from water-bearing faults in subsea tunnel based on cusp catastrophe model," *KSCE Journal of Civil Engineering*, vol. 21, no. 7, pp. 2607–2614, 2017.

[36] J. Sun and L. G. Wang, "Floor fault water-inrush prediction based on catastrophe analysis of micro-seismic signals," *Journal of china coal society*, vol. 38, pp. 1404–1410, 2013.